Geomechanics and Engineering, *Vol. 17, No. 2 (2019) 215-225*
DOI: https://doi.org/10.12989/gae.2019.17.2.215

Mechanical and acoustic behaviors of brine-saturated sandstone at elevated temperature

Yan-Hua Huang[1,2a] and Sheng-Qi Yang[*1]

[1]*State Key Laboratory for Geomechanics and Deep Underground Engineering, School of Mechanics and Civil Engineering, China University of Mining and Technology, Xuzhou 221116, P.R. China*
[2]*School of Resources and Geosciences, China University of Mining and Technology, Xuzhou 221116, P.R. China*

(Received October 11, 2018, Revised January 7, 2019, Accepted January 22, 2019)

Abstract. The mechanical behavior of rock is essential to estimate the capacity and long-term stability of CO_2 storage in deep saline aquifers. As the depth of reservoir increases, the pressure and temperature that applied on the rock increase. To answer the question of how the confining pressure and temperature influence the mechanical behavior of reservoir rock, triaxial compression experiments were carried out on brine-saturated sandstone at elevated temperature. The triaxial compressive strength of brine-saturated sandstone was observed to decrease with increasing testing temperature, and the temperature weakening effect in strength enhanced with the increase of confining pressure. Sandstone specimens showed single fracture failures under triaxial compression. Three typical regions around the main fracture were identified: fracture band, damaged zone and undamaged zone. A function was proposed to describe the evolution of acoustic emission count under loading. Finally, the mechanism of elevated temperature causing the reduction of strength of brine-saturated sandstone was discussed.

Keywords: sandstone; elevated temperature; strength; acoustic emission; ultrasonic velocity

1. Introduction

CO_2 capture and sequestration aims to reduce further increases in anthropogenic greenhouse gas emissions during the transition to a low carbon global economy over the next few decades. Geological sequestration of CO_2 in sedimentary formations, for example deep saline aquifers, is considered as an effective large-scale storage solution (Bachu *et al.*, 2003). As stated by Vulin *et al.* (2012), it is no need to further evaluate a sequestration site if the strength of cap rock is insufficient to persist poro-elastic effects caused by changes in pore fluid pressure. The mechanical properties of rock can be modified due to the geochemical interaction and therefore threaten the integrity (Lamy-Chappuis *et al.*, 2016). Therefore, the mechanical behavior of rock is a key parameter in the estimation of CO_2 storage capacity and long-term safty of gelogical CO_2 sequestration project.

Many laboratory studies have been carried out to investigate the mechanical response of rock in the presence of saline fluid. For example, Liang *et al.* (2012) conducted uniaxial compression tests on gypsum specimens that were immersed with NaCl solutions. After being soaking in brine under different conditions, reductions in both strength and elasctic modulus were clearly observed, compared with the dry specimens. Nasvi *et al.* (2014) tested the geopolymer (G), sandstone (S) and G-S composite wellbore materials under uniaxial compression to explore the influences of brine concentration and curing time on the mechanical parameters of these materials. Three salinities of the solution (0%, 5% and 15 NaCl) and four periods for saturation (14, 30, 60 and 90 days) were investigated in their study. The results showed that the strength reduction rates of G and G-S specimens in 15% NaCl were less than those in 0% and 5% NaCl, while the strength reduction of S specimens kept constant regardless of the solution medium. Lu *et al.* (2014) carried out several uniaxial compression tests on sandstone specimens which were saturated by NaCl soulution with different pH values. From their experimental results, one could observe that acidic and akiline solutions not only reduced the strength of sandstone, but also accelerated the initiation of primary crack. To study the effects of NaCl concentration and confining pressure on the mechanical properties, ultrasonic velocity and acoustic emission (AE) of rock, Huang *et al.* (2018) performed a series of conventional triaxial compression tests on sandstone specimens. Their experimental results revealed that both brine concentration and confined stress exhibited positive correlation to the peak strength, the damage stress, the elastic modulus, the cohesion, the internal friction angle, the P-wave velocity and the AE count of the tested sandstone specimen.

Potential saline aquifers for CO_2 storage are often located more than 800 m below the earth surface (Bruant *et al.*, 2002), and therefore underground resevoir rocks are suffered from the elevated temperature due to the geothermal gradient (Yan *et al.* 2017, Huang *et al.* 2017, Yang *et al.* 2017 and 2018). For instance, the mean temperature of Sherwood Sandstone Group was 50°C at

*Corresponding author, Professor
E-mail: yangsqi@hotmail.com
[a]Ph.D.
E-mail: huangyh1219@163.com

http://www.techno-press.org/?journal=gae&subpage=7
ISSN: 2005-307X (Print), 2092-6219 (Online)

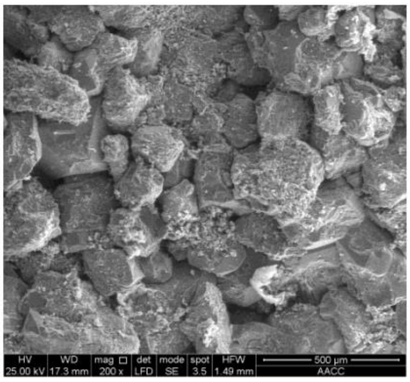

(a) Scanning electron microscope (SEM) image

(b) Optical microscope image

Fig. 1 Micro structure of the tested sandstone

depths from 1100 m to 1498 m in the East Yorkshire and Lincolnshire Basin, UK (Downing *et al.* 1985, Hall *et al.* 2016), and the virgin temperature of reservoir unit in the In Salah onshore saline aquifer (central Algeria) was 93 °C (Hosa *et al.* 2010, Beni and Clauser 2014). To increase the understanding of strength and deformation behavior of rock in deep saline aquifers, elevated temperature effect should be taken into acount. Experimental results of water-saturated rock specimens at elevated temperature have been reported by Inada *et al.* (1997) and Pei *et al.* (2016). Masuda *et al.* (2012) conducted conventional triaxial compression tests on dry and wet mylonite specimens at high temperature to study the change of mechanical properties of rock in the presence of water. As the temperature increased, the frictional strength of wet mylonite specimen decreased, but that of dry specimen changed slightly. Lisabeth and Zhu (2015) investigated the coupled mechanical, thermal and chemical processes by conducting triaxial compression tests on limestone specimen. They observed from the experiments that water weakening effect in strength was sensitive to fluid composition and temperature. What is more important was that limestone specimens that saturated with equilibrated fluids ($CaCO_3$ used in the test) were stronger than those with distilled water. As reported by Korsnes *et al.* (2008), the mechanical properties of chalk specimens exhibited significantly different response to distilled water and seawater at elevated temperature. The studies of Lisabeth and Zhu (2015) and Korsnes *et al.* (2008) showed that chemical reaction between rock and pore fluid played an important role in the mechanical behavior of rock at elevated confining pressure and temperature environment. How do brine and elevated temperature influence the mechanical behavior of rock? The answer is very essential for the evaluation of a deep saline aquifer for CO_2 storage. Additionally, the ultrasonic and AE behaviors of rock at elevated teperatures have not been fully investigated. Therefore, in this study, triaxial compression tests at elevated temperature were carried out on brine-saturated sandstone for a range of temperatures (20-90°C) and confining pressures (10-60 MPa). During the triaxial deformation tests, ultrasonic and AE monitoring techniques, which are effective non-destructive methods for prediction of physical and mechanical behaviors of rocks (Abdelhedi *et al.* 2017), were used to detect the P-wave velocity and AE counts. Finally, the mechanism of the elevated temperature causing the mechanical properties weakening of sandstone was discussed.

2. Experimental methodology

CO_2 is always injected into sandstone reservoirs in deep saline aquifers due to its relatively high porosity and permeability. Sandstone was therefore chosen as the tested rock throughout this research, which was collected from Zunyi City of Guizhou Province, China. The sandstone had a good homogeneity that allowed us to run repeat tests with minimal variation. The porosity of the sandstone was 16.2% according to the mercury intrusion porosimetry test. The average density of the sandstone was 2130 kg/m^3 (Huang *et al.* 2018). The micro structure of the tested sandstone specimen is shown in Fig. 1. X-ray diffraction analysis showed that the mineral components were mainly quartz (95.8%) and minor quantities of feldspar, dolomite and clay minerals (Huang *et al.*, 2019).

2.2 Specimen preparation

Sandstone cylinders with 50 mm in diameter and 100 mm height were cored from one block of sandstone. The ratios of height to diameter was 2:1 and met the suggested range of International Society for Rock Mechanics and Rock Engineering (Fairhurst and Hudson 1999). Both the two ends of specimens were polished to minimize the end-friction effects. Then sandstone specimens were placed in a desiccator filled with brine under vacuum for 60 days. A NaCl solution was used to replace with reservoir water in this study. The salinity of brine was 20 wt. %, i.e., 100 g distilled water dissolved with 20 g pure NaCl crystals. The detailed saturation procedure can be referred in Yang *et al.* (2018).

2.3 Experimental configuration

A rock mechanics servo testing system (Model GCTS RTX-4000, GCTS Testing Systems, Tempe, AZ, USA) was used for triaxial compression tests. The overview of the

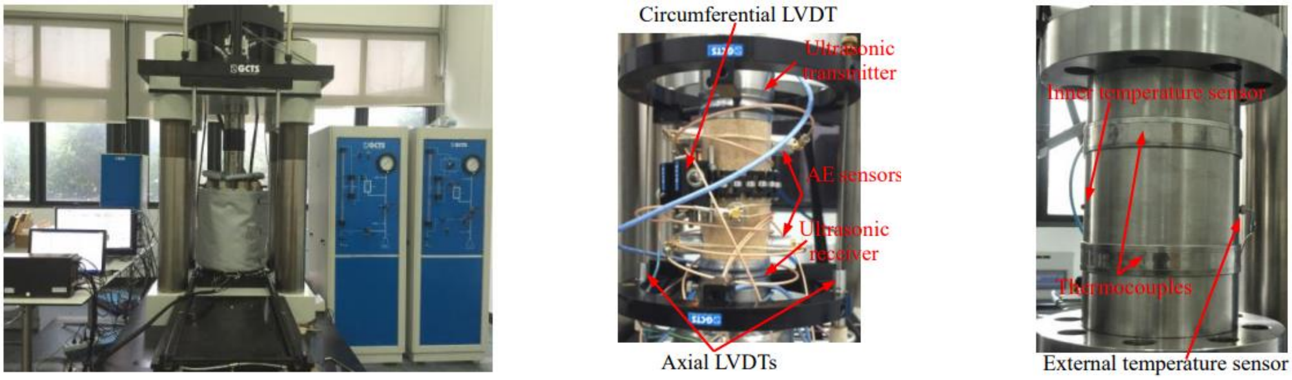

(a) GCTS testing system (b) Deformation, ultrasonic and AE measurements (c) Temperature controller

Fig. 2 Experimental apparatus used in this experiment

GCTS testing system is shown in Fig. 2(a), which consisted of a triaxial cell, a hydraulic station, a pore pressure pump and a confining pressure pump. The capacities for the axial loading, pore pressure and confining pressure were 4000 kN, 140 MPa and 140 MPa, respectively. Deformations were measured by using the external linear variable differential transducers (LVDTs). As shown in Fig. 2(b), axial deformation was measured by two axial LVDTs which were symmetrically mounted on two sides of the specimen, and lateral deformation was measured by a circumferential LVDT which was located in the middle part of the specimen to reduce the end-friction effect.

Elevated temperature was applied on the rock specimen via two external thermocouples, which were ring shapes symmetrically wrapped around the triaxial cell (Fig. 2(c)). A temperature of 150°C was the highest value drived by the temperature control system. The triaxial cell was filled with silicone oil, which acted as confining pressure and temperaure evironment. Two temperature sensors were used to measure the internal (i.e., the specimen) and external (i.e., the wall of the cell) temperature. The measured inner temperature was used as feedback to control the temperature in real-time.

To explore the AE characteristics in rock specimen at elevated temperature, a micro-II AE measuring system (Physical Acoustic Corporation, Princeton, NJ, USA) was used during the whole deformation process in this experiment. AE sensors were installed on the surface of the specimen instead of the triaxial cell (see Fig. 2(b)). To further detect the damage of sandstone under stress, P-wave along the axial direction was recorded with an ultrasonic pulse transmission technique. The transmitter was positioned on the top end surface and the receiver was put on the bottom end surface of the specimen (see Fig. 2(b)); an electric pulse was generated with a pulse generator, and the waveforms were recorded using a digital oscilloscope (Huang *et al.* 2018).

2.4 Testing procedure

First, the brine-saturated sandstone specimens were placed inside the triaxial cell. Confining pressure was increased to the desired value at a low stress rate of 4.0 MPa/min and kept constant during the entire triaxial compression. Second, silicone oil was heated to the target temperature at a very low rate of approximate 0.75°C/min to avoid thermal damage on rock specimen. Before the next step, the temperature was maintained for 2 h to ensure uniformity in temperature across the rock specimen. Third, axial stress was loaded on the surface of specimen at a displacement rate of 0.04 mm/min untill failure took place. During the loading, the testing temperature was kept constant, and the loads, displacements, ultrasonic and AE information were recorded simultaneously.

In this test, the confining pressure range was 20-60 MPa, and the temperature range was 20-90°C, which could be used to simulate the influence of reservoir depths. The maximum values of confining pressure and temperature corresponded to the maximum reservoir depth of 2400 m, assuming a reservoir rock density of 2500 kg/m^3 and a thermal gradient of 30°C/km.

3. Results and analysis

3.1 Stress-strain relationship

Fig. 3 shows the axial deviatoric stress-axial strain curves of brine-saturated sandstone specimens at elevated temperature. The curves at room temperature (i.e., 20 °C) in this figure were collected from Huang *et al.* (2018). The shapes of the stress-strain relationships at elevated temperature were almost the same as those at room temperature. They all underwent an initial compaction, elastic deformation, nonlinear deformation, abrupt post-peak failure and residual strength stages. At low confining pressures, the initial compaction stage was obvious, but it reduced gradually, as the confining pressure increased, which was a result of denser grain assembly at higher confining pressure. Under the same confining pressure, the testing temperature had an influence on the stress-strain response, and this temperature effect enhanced with increasing confining pressure.

Fig. 4 shows the volumetric strain- axial strain curves of brine-saturated sandstone specimens at elevated temperature. The volumetric strain was calculated by axial

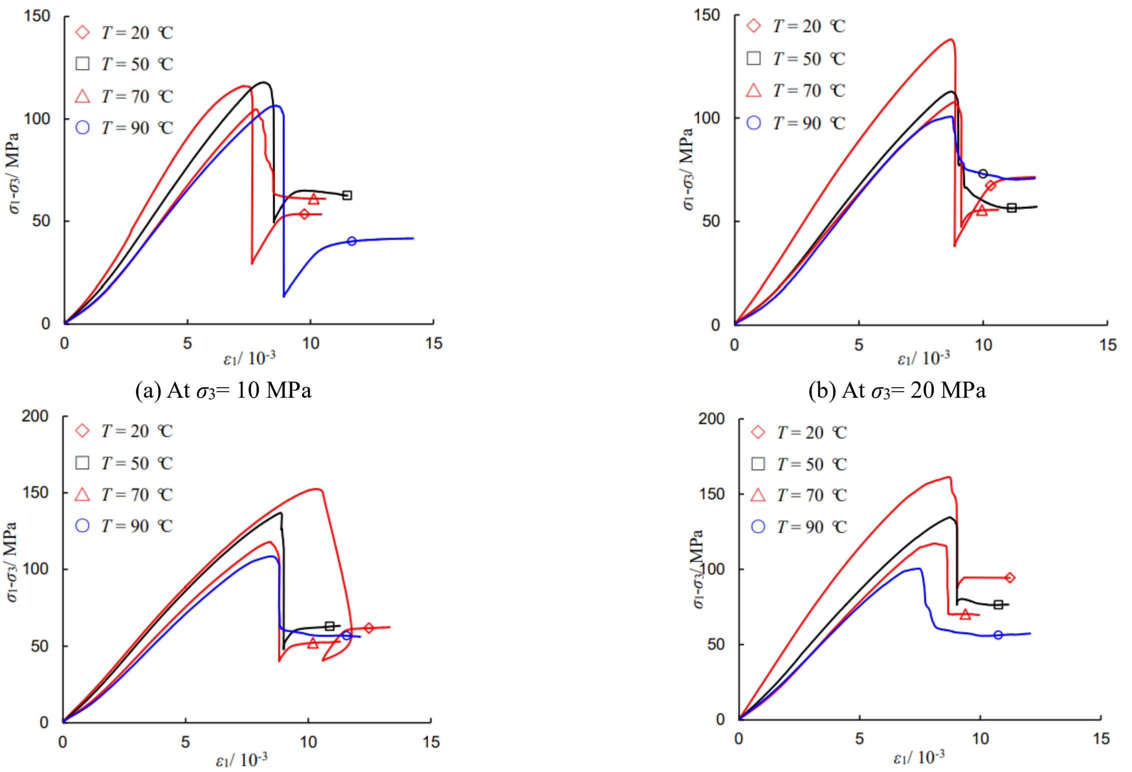

(a) At σ_3= 10 MPa (b) At σ_3= 20 MPa

(c) At σ_3= 40 MPa (d) At σ_3= 60 MP

Fig. 3 Axial deviatoric stress-strain curve of brine-saturated sandstone at elevated temperature

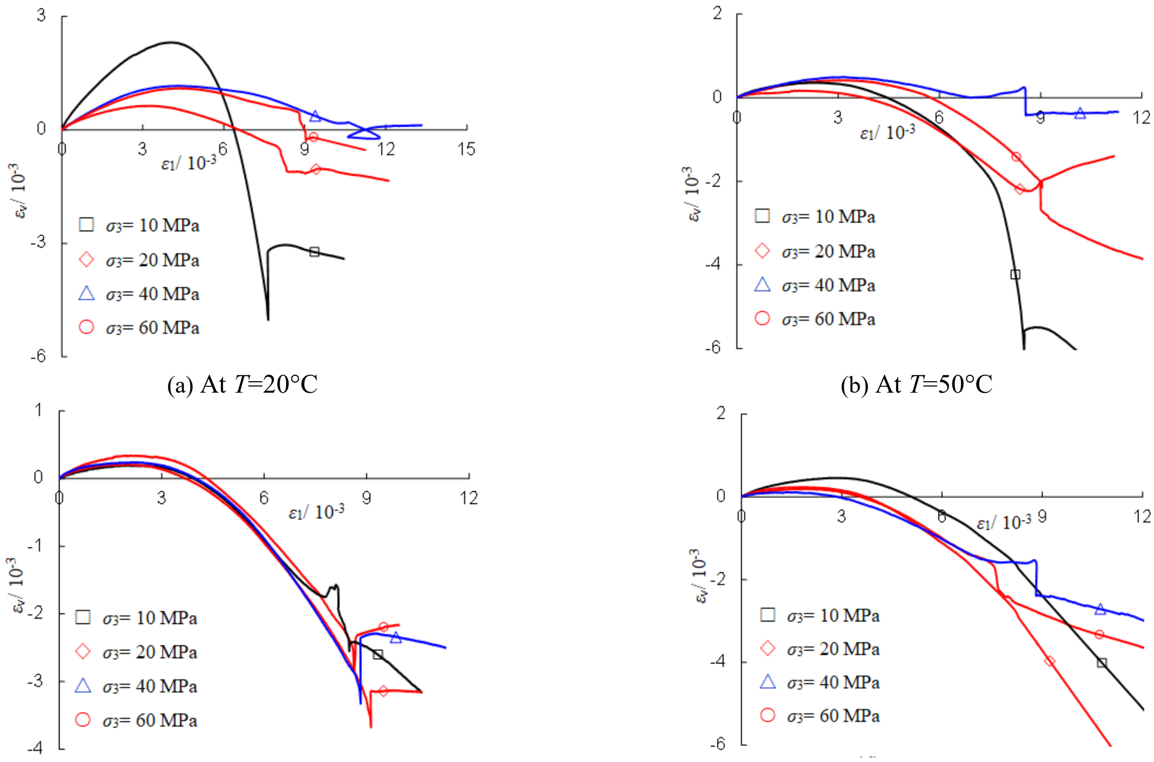

(a) At T=20°C (b) At T=50°C

(c) At T=70°C (d) At T=90°C

Fig. 4 Volumetric strain-axial curves of brine-saturated sandstone specimens at elevated temperature

strain and twice lateral strains. The volumetric strain was initially positive and increased with the axial strain, indicating that the rock specimen was compressed continuously under external stress. When the peak was reached, the volumetric strain displayed a reverse trend. The volumetric strain decreased with the axial strain. It implies

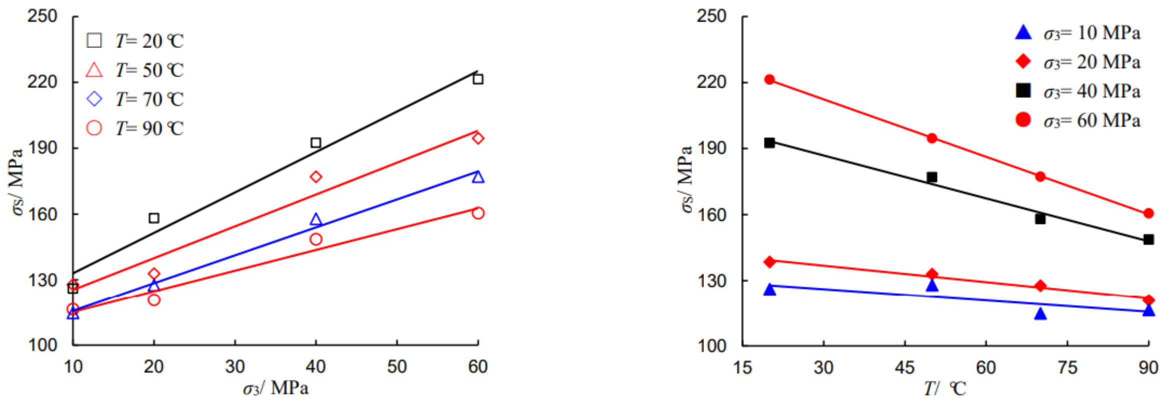

(a) Influence of confining pressure (b) Influence of testing temperature

Fig. 5 Peak strengths of brine-saturated sandstone specimens at elevated temperature

that the rock specimen changed from compaction-dominated to dilation-dominated.

3.2 Peak strength

On the basis of stress-strain curves, the peak strengths of sandstone specimens with respect to various testing temperatures are listed in Table 1. σ_p represents the peak deviatoric stress, and σ_S represents the peak strength, which is calculated by σ_p pluses σ_3.

Fig. 5 shows the influences of confining pressure and testing temperature on the peak strength of brine-saturated sandstone specimens. As the confining pressure increased, the peak strength of brine-saturated sandstone was observed to increase (Fig. 5(a)). However, the peak strength exhibited a negative relation to the testing temperature. It is seen from Fig. 5(b) that the peak strength decreased linearly with the increase of temperature. The relationships between strength and temperature are expressed as Eq. (1).

$$
\begin{aligned}
\sigma_S &= -0.17T + 131.30 \ (\sigma_3 = 10\ \text{MPa}) \\
\sigma_S &= -0.25T + 144.28 \ (\sigma_3 = 20\ \text{MPa}) \\
\sigma_S &= -0.65T + 206.43 \ (\sigma_3 = 40\ \text{MPa}) \\
\sigma_S &= -0.87T + 238.48 \ (\sigma_3 = 60\ \text{MPa})
\end{aligned} \tag{1}
$$

Table 1 Peak strengths of brine-saturated sandstone

Specimen	σ_3/MPa	T/°C	σ_p/MPa	σ_S/MPa
ZY-A-57[a]	10	20	116.02	126.02
ZY-A-64[a]	20	20	138.11	158.11
ZY-A-50[a]	40	20	152.48	192.48
ZY-A-51[a]	60	20	161.36	221.36
ZY-A-77	10	50	117.85	127.85
ZY-A-74	20	50	112.90	132.90
ZY-A-67	40	50	136.98	176.98
ZY-A-66	60	50	134.57	194.57
ZY-A-89	10	70	104.75	114.75
ZY-A-56	20	70	107.65	127.65
ZY-A-60	40	70	117.91	157.91
ZY-A-59	60	70	117.17	177.17
ZY-A-72	10	90	106.40	116.40
ZY-A-70	20	90	100.74	120.74
ZY-A-62	40	90	108.61	148.61
ZY-A-71	60	90	100.49	160.49

Note: Data [a] was collected from Huang *et al.* (2018)

3.3 Macro and micro fractures

The ultimate failure modes of brine-saturated sandstone specimens at elevated temperature are shown in Fig. 6. The failed specimen at room temperature was presented by Huang *et al.* (2018). All the tested sandstone specimens failed with a main shear fracture and local minor cracks. Many sands were observed from the shear fracture, which resulted from the friction between the upper and lower fracture planes. In the range of the testing conditions, both temperature and confining pressure did not show significant influence on macro failure patterns, because the maximum testing confining pressure was insufficient to change the failure mode (Fang and Harrison 2002).

To characterize the shear fracture, X-ray computer tomography (CT) scanning was conducted by using a Nanotom 160 high-resolution micro-CT with a spatial resolution of 30 μm. Two representative three dimensional (3D) reconstruction results are shown in Fig. 6d. The scanning region was 50 mm in diameter and 68 mm in height. Fracture regions with lower CT numbers are black, and other regions with relatively higher CT numbers are transparent. The apparent shear fracture displayed as a rough curved surface in 3D space. At different heights, the shear fracture showed different patterns. Crack propagated toward the direction of thickness, indicating that 3D crack was more complicated than two dimensional (2D) crack (Dyskin *et al.*, 2003).

The analysis of local fracture characteristics enhanced the understanding of rock mechanical behavior (Baud *et al.* 2015). Theoretically, SEM is effective for the micro structure observation because it has a higher spatial resolution (Zhou *et al.* 2018). However, grains and micro cracks are not easily distinguishable in a typical dark gray and black SEM image (Cheng *et al.* 2016). Mineral grains and micro cracks can be presented in different colors under optical microscope, which makes them easily to be identified.

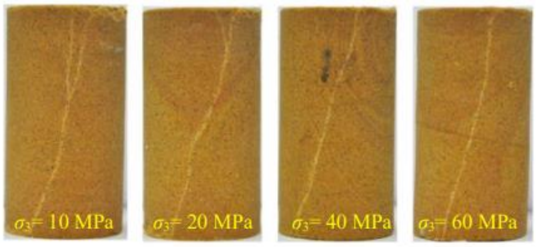

(a) At T=50°C

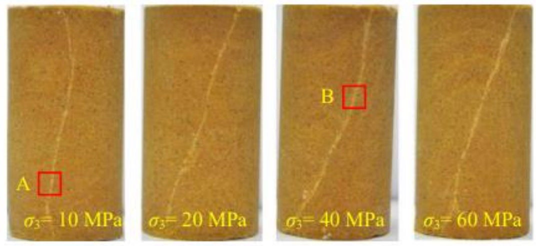

(b) At T=70°C

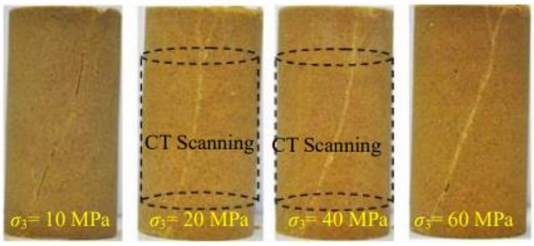

(c) At T=90°C

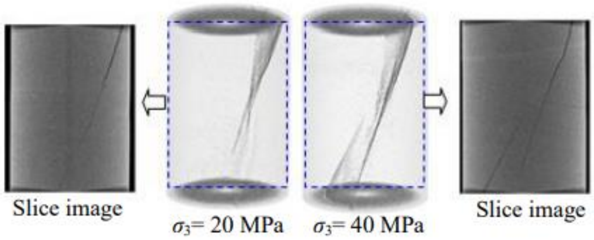

(d) CT reconstruction (T =90°C)

Fig. 6 Ultimate failure modes of brine-saturated sandstone specimens at elevated temperature

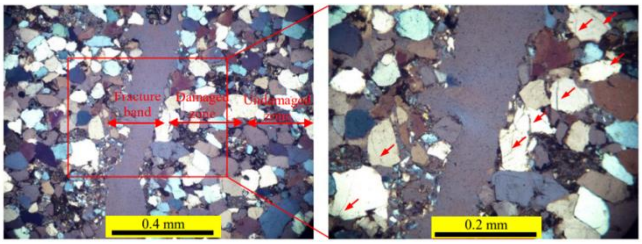

Fig. 7 Local characteristic of a fracture in a brine-saturated sandstone (T=70 °C, σ_3=10 MPa)

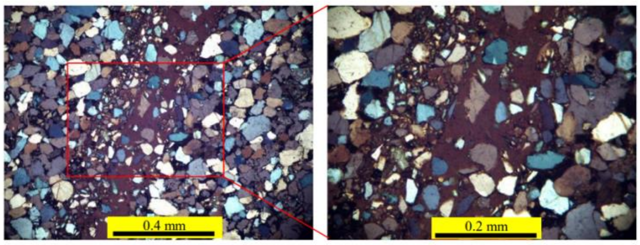

Fig. 8 Local characteristic of a fracture in a brine-saturated sandstone (T=70 °C, σ_3=40 MPa)

Therefore, an optical microscope (Model DYP-990C, Shanghai Dianying Optical Instrument Co., Ltd., Shanghai, China) was used to detect the local fracture behavior of brine-saturated sandstone after failure. Two representative results collected from the failed specimens at T=70°C (as the marked A and B in Fig. 6(b)) under confining pressures of 10 and 40 MPa are shown in Figs. 7 and 8, respectively. In these images, the main fractures were located in the center with dark gray color.

At σ_3= 10 MPa, the selected main fracture was almost parallel to the loading direction. The fracture was a rough and irregular crack, and had different widths in different positions. This indicates the heterogeneity effect on the micro structure of rock. Many fractured grains were observed near the main fracture. The grains close to the fractured ones kept relatively intact, but transgranular cracks were initiated in these grains. However, micro cracks died far away from the main fracture. Three typical regions were identified: fracture band, damaged zone and undamaged zone (Fig. 7). These micro observations were similar with the results in the past studies (Vajdova *et al.* 2004, Ingraham *et al.* 2017). When the confining pressure increased to 40 MPa, more fractured grains were observed in and near the main fracture (Fig. 8). It implies that more transgranular cracks were initiated under a higher confining pressure.

3.4 P-wave velocity evolution characteristics

Fig. 9 shows the evolution processes of P-wave velocity in brine-saturated sandstone specimens at elevated temperature. From Fig. 9(a), P-wave velocity was observed to increase with increasing confining pressure under the same testing temperature, resulting from the densification of the particle assembly within the rock under increased confining pressure (Huang *et al.* 2018). However, from Fig. 9(b), the testing temperature in the present study showed no significant influence on the evolution of P-wave velocity, which was consistent with the previous study (Kern and Tubia 1993).

The variation trends of P-wave velocity of brine-saturated sandstone specimens were similar with respect to different confining pressures and testing temperatures. The basic law for P-wave velocity is summarized as follows: At the low stress level, the ultrasonic velocity increased with the axial stress, which was closely related to the closure of micro cracks. At the elastic deformation stage, the ultrasonic velocity continued to increase with the axial stress, because the P-wave velocity was positively related to the density of rock material (Zhou *et al.* 2016). However, many fluctuations in the ultrasonic velocity curve were observed, which mainly resulted from the initiation and propagation of cracks. Reverse in the ultrasonic velocity occurred prior to the peak strength, indicating that the structure of the specimen was damaged. At the stress softening stage, the ultrasonic velocity decreased with the

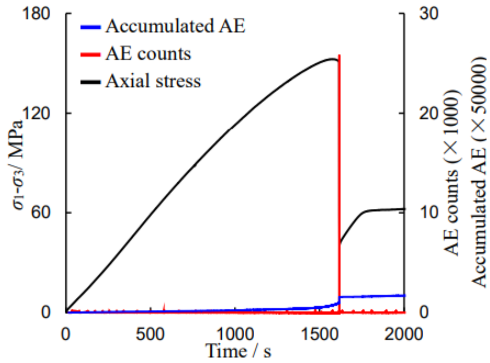

(a) σ_3=40 MPa, T=20°C

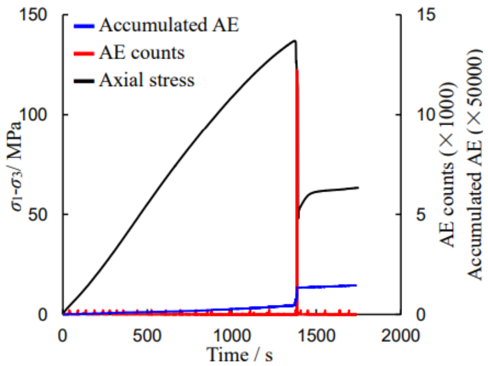

(b) σ_3=40 MPa, T=50°C

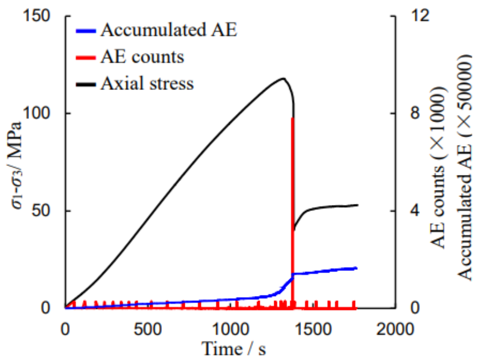

(c) σ_3=40 MPa, T=70°C

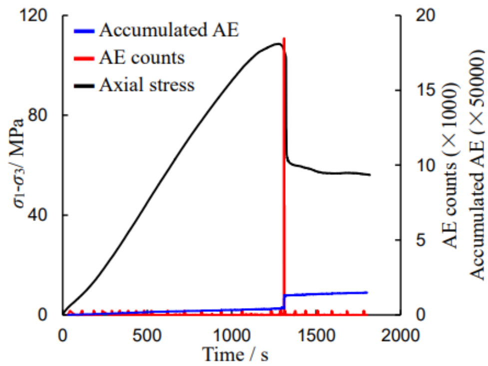

(d) σ_3=40 MPa, T=90°C

Fig. 10 Effect of elevated temperature on AE counts of brine-saturated sandstone

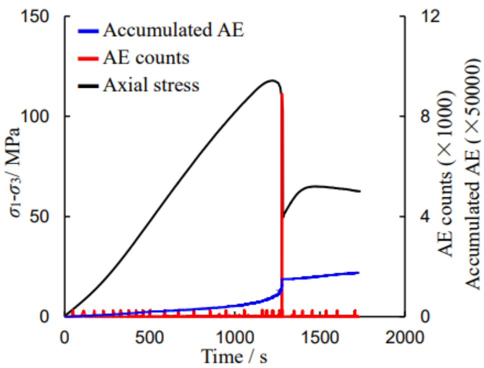

(a) σ_3=10 MPa, T=50°C

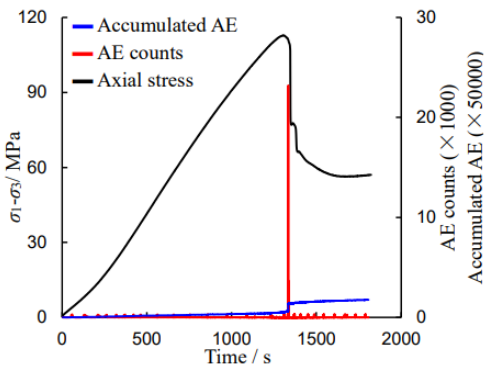

(b) σ_3=20 MPa, T=50°C

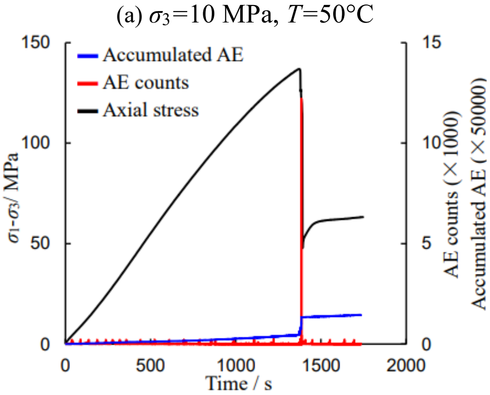

(c) σ_3=40 MPa, T=50°C

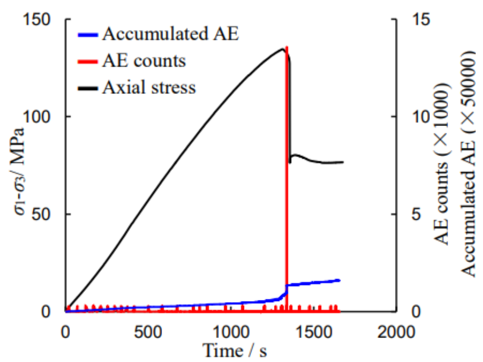

(d) σ_3=60 MPa, T=50°C

Fig. 11 Effect of confining pressure on AE counts of brine-saturated sandstone

decrease of the axial stress. The observations of evolution process of ultrasonic velocity were in agreement with the previous studies (Liu *et al.* 2017, Stanchits *et al.* 2006).

Furthermore, the ultrasonic velocity at the post-peak stage was higher than the initial value. It indicates that the P-wave velocity did not attenuate seriously caused by the

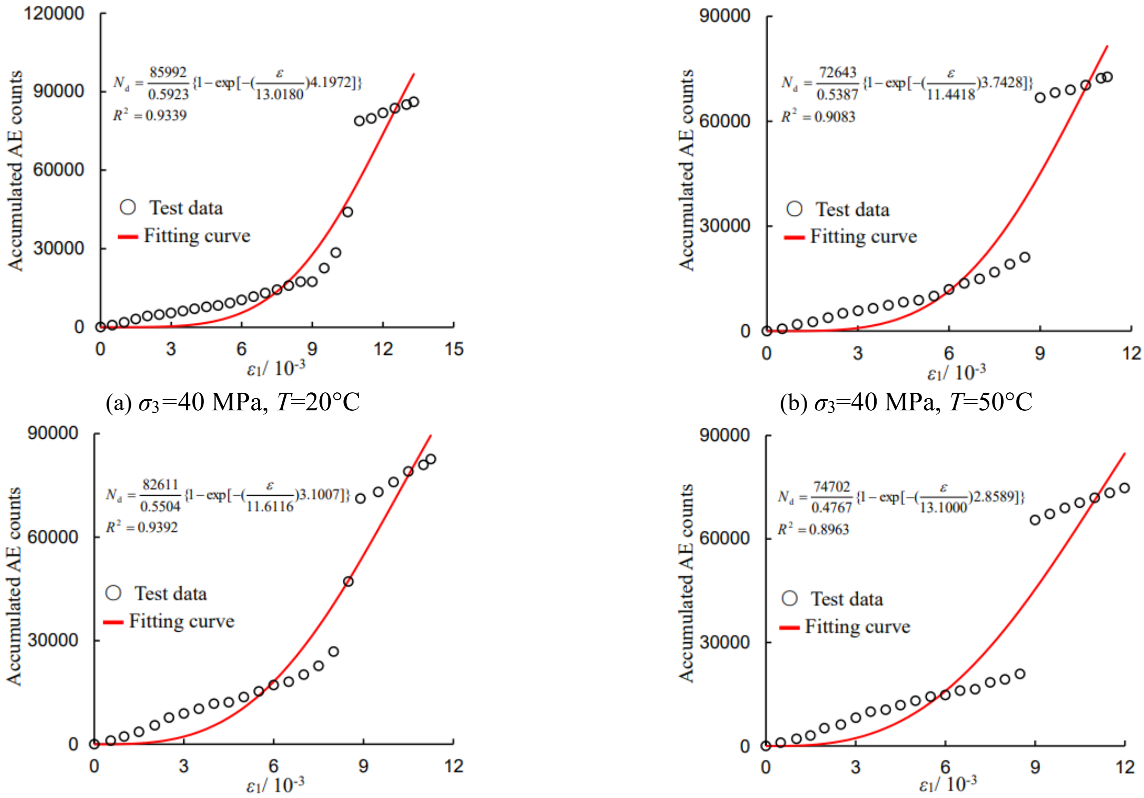

(a) σ_3=40 MPa, T=20°C (b) σ_3=40 MPa, T=50°C

(c) σ_3=40 MPa, T=70°C (d) σ_3=40 MPa, T=90°C

Fig. 12 Accumulated AE counts and fitting curves of sandstone at elevated temperature

macro fracture under triaxial compression. The measured P-wave was along the axial direction (see Fig. 2(b)) and the vibration direction of particle of P-wave was parallel to the propagation direction. However, the angle between the main fracture and axial direction was small (see Fig. 6), which reduced the influence of main fracture on the decrement of P-wave velocity.

3.5 AE evolution characteristics

Figs. 10 and 11 show the evolution of AE count of brine-saturated sandstone during the whole deformation process. The overall trends of AE count were similar for different confining pressures and testing temperatures. Under triaxial compression, most of the energy was accumulated before the peak strength, and released after failure. The most active period in AE count curve was observed at the post-peak failure moment, and a corresponding sudden increase was seen in the accumulated AE count curve. The maximum AE count column was 10~20 times of others. Both the confining pressure and testing temperature showed no significant influence on the evolution of AE count in brine-saturated sandstone specimen. The AE count curves at elevated temperature were a little different to those under uniaxial compression (Wu *et al.* 2018, Xu *et al.* 2013), where multiple large AE counts were clearly observed at pre-peak stage. Mesoscopic damage in rock distributes randomly. Generally, empirical Weibull function is effective to study the distribution of mesoscopic damage, whose probability density function (Tang 1993) can be formulated by Eq. (2).

$$\varphi(\varepsilon) = \frac{m}{\varepsilon_0}\left(\frac{\varepsilon}{\varepsilon_0}\right)^{m-1}\exp\left[-\left(\frac{\varepsilon}{\varepsilon_0}\right)^m\right] \tag{2}$$

where, $\varphi(\varepsilon)$ is the density function, m is the shape parameter, ε_0 is the scale parameter of the distribution, and ε is the strain of mesoscopic element.

From Eq. (2), the distribution function of meso unit failure can be expressed as Eq. (3).

$$F(\varepsilon) = \int_0^\varepsilon \varphi(\varepsilon)\mathrm{d}\varepsilon = \int_0^\varepsilon \frac{m}{\varepsilon_0}\left(\frac{\varepsilon}{\varepsilon_0}\right)^{m-1}\exp\left[-\left(\frac{\varepsilon}{\varepsilon_0}\right)^m\right]\mathrm{d}\varepsilon = 1-\exp\left[-\left(\frac{\varepsilon}{\varepsilon_0}\right)^m\right] \tag{3}$$

Damage variable (D) is a concept to describe the extent of meso damage, which has a relationship with probability density function, as shown in Eq. (4).

$$\frac{dD}{d\varepsilon} = \varphi(\varepsilon) \tag{4}$$

Then the damage variable D can be obtained as follows

$$D = 1-\exp\left[-\left(\frac{\varepsilon}{\varepsilon_0}\right)^m\right] \tag{5}$$

where, σ_{cr} is the residual strength, and σ_p is the peak strength.

Following the method reported by Kachnnov *et al.* (1992, 1994), damage variable D is defined

$$D = \frac{A-A_1}{A} = \frac{A_d}{A} \tag{6}$$

where, A is the whole area of rock, A_1 is the effective area (undamaged zone), and A_d is the damaged area. However, in laboratory experiment, rock specimen does not fail completely when the loading is stopped. Eq. (6) can be revised by introducing a coefficient (Darabi *et al.* 2012). Therefore, the revised damage variable can be described as

$$D = D_{\mathrm{u}} \frac{A_{\mathrm{d}}}{A} \tag{7}$$

where, D_u is an influence coefficient. Based on the study of Liu *et al.* (2009), D_u can be calculated from the following equation.

$$D_{\mathrm{u}} = 1 - \frac{\sigma_{\mathrm{cr}}}{\sigma_{\mathrm{p}}} \tag{8}$$

Assume the total AE counts is N_m when the whole rock (A) fails. When the damaged area is A_d, the accumulated AE counts are N_d. Therefore, the damage variable can be obtained from the AE counts.

$$D = D_{\mathrm{u}} \frac{N_{\mathrm{d}}}{N_{\mathrm{m}}} \tag{9}$$

In accordance with Eqs. (5), (8) and (9), the relationship between accumulated AE counts and axial strain can be written as

$$N_{\mathrm{d}} = \frac{N_{\mathrm{m}} D}{D_{\mathrm{u}}} = \frac{N_{\mathrm{m}}}{1 - \frac{\sigma_{\mathrm{cr}}}{\sigma_{\mathrm{p}}}} \{1 - \exp[-(\frac{\varepsilon}{\varepsilon_0})^m]\} \tag{10}$$

Fig. 12 shows the comparison between the experimental result and the fitting curve for different testing temperatures. In the laboratory experiment, fracture formed abruptly at the post-peak stage, leading to a sudden increase in the accumulated AE counts. Overall, the fitting curve was in agreement with the experimental result, which indicates that the proposed function of AE count produced the experimental results.

4. Discussion

4.1 Mechanism of elevated temperature in altering rock strength

Experimental results showed that the strength of brine-saturated sandstone decreased with the testing temperature. Previous study indicated that temperature altered the intensity of fluid-rock interaction (Wang *et al.* 2018). It can be inferred that the micro pore structure of sandstone was weakened at elevated temperature, which was a result of brine and temperature coupled weakening effect.

The main minerals of the tested sandstone were quartz (see Fig. 1). Theoretically, quartz was dissolved into brine solution, as described in Eq. (11). Dissolution reaction of mineral was closely related to the composition and pH of solution, interaction time, temperature and pressure. Quartz dissolution reaction was not expected to occur with neutral brine solution in a short-time.

$$SiO_2 + 2H_2O = H_4SiO_4 \tag{11}$$

The reaction should be focused on the clay minerals, because the main clay minerals of the tested sandstone was kaolinite. As known to us, kaolinite was very easily dissolved in solution (Carroll *et al.* 2011), which can be expressed as Eq. (12).

$$Al_2Si_2O_5(OH)_4 + 6H^+ = 5H_2O + 2Al^{3+} + 2SiO_2 \tag{12}$$

Previous study found that the corrosion damage ratio of gypsum in brine solution gradually increased with a rising temperature (Yu *et al.* 2016). In particular, the dissolution of kaolinite was dependent on the testing temperature (Ganor *et al.* 1995). As the temperature of solution increased, the time for kaolinite dissolution reduced (Carroll and Walther, 1990). The rate of dissolution generally follows the classical Arrhenius equation (Carroll and Walther, 1990), as written below.

$$Rate = A' \exp^{\frac{-Ea}{RT}} \tag{13}$$

where, A' is the pre-exponential factor, E_a is the apparent activation energy, R is the gas constant and T is the temperature. From Eq. (13), the rate of dissolution of kaolinite increased with the increase of temperature. The pore structure was weakened and therefore the strength decreased as the testing temperature increased.

4.2 Implication and future study

The strength of brine-saturated sandstone was observed to decrease with increasing temperature, and the rate of decrement increased under higher confining pressure. It indicates that as the depth of reservoir increases (both the temperature and confining pressure increase), the strength of reservoir rock in deep saline aquifer decreases. From the perspective of rock engineering, it influences the stability and safety of underground project. It suggests that engineers should pay attention to the mechanical response of reservoir rock when selecting a CO_2 sequestration site.

The potential geological media for geological CO_2 sequestration must have the following three characteristics: capacity, injectivity and confinement (Bachu, 2008). The mechanical parameter reduction results from the weakening in pore structure. The permeability and porosity of rock will increase due to the rock-water interaction (e.g., dissolution of mineral). From the perspective of CO_2 injectivity, it is beneficial for CO_2 injection.

However, this study was carried out on brine-saturated sandstone with selected confining pressure and temperature conditions. The experimental results can be regarded as a reference for future studies of mechanical behavior of rock in deep saline aquifer after CO_2 injection. The interaction within brine-CO_2-rock is not well understood and should be the emphasis of future study.

5. Conclusions

• The stress-strain curves and peak strength of brine-saturated sandstone were influenced by the confining pressure and testing temperature. As the testing temperature increased, the peak strength of brine-saturated sandstone specimen decreased. Furthermore, the temperature weakening effect in strength increased with the increase of confining pressure.

• All the brine-saturated sandstone specimens exhibited single shear failure modes for a range of confining pressures (10-60 MPa) and temperatures (20-90°C). On the viewpoint of macroscopic, the testing confining pressure and temperature had no significant influence on the failure pattern. On the viewpoint of microscopic, three typical regions were identified: fracture band, damaged zone and undamaged zone.

• The P-wave velocity of sandstone was related to the confining pressure, but independent to the testing temperature. The confining pressure enhanced the P-wave velocity of sandstone specimen. The AE count exhibited a similar evolution trend under different confining pressures and testing temperatures. A function based on Weibull distribution was proposed to describe the evolution of AE count under loading.

Acknowledgements

The research described in this paper was financially supported by the National Postdoctoral Program for Innovative Talents (BX20180359). The authors would like to express their sincere gratitude to the editor and anonymous reviewer for their valuable comments, which have greatly improved this paper.

References

Abdelhedi, M., Aloui, M., Mnif, T. and Abbes, C. (2017), "Ultrasonic velocity as a tool for mechanical and physical parameters prediction within carbonate rocks", *Geomech. Eng.*, **13**(3), 371-384.

Bachu, S. (2003), "Sequestration of CO_2 in geological media in response to climate change: capacity of deep saline aquifers to sequester CO_2 in solution", *Energy Convers. Manage.,* **44**(20), 3151-3175.

Bachu, S. (2008), "CO_2 storage in geological media: Role, means, status and barriers to deployment", *Prog. Energy Combust. Sci.*, **34**(2), 254-273.

Baud, P., Reuschlé, T., Ji, Y., Cheung, C.S.N. and Wong, T. (2015), "Mechanical compaction and strain localization in Bleurswiller sandstone", *J. Geophys. Res. Solid Earth*, **120**(9), 6501-6522.

Beni, A.N. and Clauser, C. (2014), "The influence of temperature on chemical fluid-rock reactions in geological CO_2 sequestration", *Environ. Model. Assess.*, **19**(4), 315-324.

Bruant, R., Guswa, A., Celia, M. and Peters, C. (2002), "Safe storage of CO_2 in deep saline aquifers", *Environ. Sci. Technol.*, **36**(11), 240A-245A.

Carroll, S.A. and Walther, J.V. (1990), "Kaolinite dissolution at 25°, 60°, and 80°C", *Am. J. Sci.*, **290**(7), 797-810.

Carroll, S.A., Mcnab, W.W. and Torres, S.C. (2011), "Experimental study of cement-sandstone/shale-brine-CO_2 interactions", *Geochem. Trans.*, **12**(1), 9.

Cheng, Y., Wong, L.N.Y. and Maruvanchery, V. (2016), "Transgranular crack nucleation in carrara marble of brittle failure", *Rock Mech. Rock Eng.*, **49**(8), 3069-3082.

Darabi, M.K., Al-Rub, R.K.A. and Little, D.N. (2012), "A continuum damage mechanics framework for modeling micro-damage healing", *Int. J. Solid. Struct.*, **49**(3-4), 492-513.

Downing, R.A., Allen, D.J., Bird, M.J., Gale, I.N., Kay, R.L.F. and Smith, I.F. (1985), *Cleethorpes No. 1 Geothermal Well–A Preliminary Assessment of the Resource: Investigation of the Geothermal Potential of the UK*, British Geological Survey.

Dyskin, A.V., Sahouryeh, E., Jewell, R.J., Joer, H. and Ustinov, K.B. (2003), "Influence of shape and locations of initial 3-D cracks on their growth in uniaxial compression", *Eng. Fract. Mech.*, **70**(15), 2115-2136.

Fairhurst, C.E. and Hudson, J.A. (1999), "Draft ISRM suggested method for the complete stress-strain curve for intact rock in uniaxial compression", *Int. J. Rock Mech. Min. Sci.*, **36**(3), 279-289.

Fang, Z. and Harrison, J.P. (2002), "Application of a local degradation model to the analysis of brittle fracture of laboratory scale rock specimens under triaxial conditions", *Int. J. Rock Mech. Min. Sci.*, **39**(4), 459-476.

Ganor, J., Mogollón, J.L. and Lasaga, A.C. (1995), "The effect of pH on kaolinite dissolution rates and on activation energy", *Geochimica Cosmochimica Acta*, **59**(6), 1037-1052.

Hall, M.R., Rigby, S.P., Dim, P., Bateman, K., Mackintosh, S.J. and Rochelle, C.A. (2016), "Post-CO_2 injection alteration of the pore network and intrinsic permeability tensor for a Permo-Triassic sandstone", *Geofluids*, **16**(2), 249-263.

Hosa, A., Esentia, M., Stewart, J. and Haszeldine, S. (2010), *Benchmarking Worldwide CO_2 Saline Aquifer Injections*, Scottish Centre for Carbon Capture and Storage, Edinburgh, Scotland, U.K.

Huang, Y.H., Yang, S.Q., Hall, M.R., Zhang, Y.C. (2018), "The effects of NaCl concentration and confining pressure on mechanical and acoustic behaviors of brine-saturated sandstone", *Energies*, **11**(2), 385.

Huang, Y.H., Yang, S.Q. and Tian, W.L. (2019), "Crack coalescence behavior of sandstone specimen containing two pre-existing flaws under different confining pressures", *Theor. Appl. Fract. Mech.*, **99**, 118-130.

Huang, Y.H., Yang, S.Q., Tian, W.L., Zhao, J., Ma, D. and Zhang, C.S. (2017), "Physical and mechanical behavior of granite containing pre-existing holes after high temperature treatment", *Arch. Civ. Mech. Eng.*, **17**(4), 912-925.

Inada, Y., Kinoshita, N., Ebisawa, A. and Gomi, S. (1997), "Strength and deformation characteristics of rocks after undergoing thermal hysteresis of high and low temperatures", *Int. J. Rock Mech. Min. Sci.*, **34**(3-4), 140.

Ingraham, M.D., Bauer, S.J., Issen, K.A. and Dewers, T.A. (2017), "Evolution of permeability and Biot coefficient at high mean stresses in high porosity sandstone", *Int. J. Rock Mech. Min. Sci.*, **96**, 1-10.

Kachanov, M. (1992), "Effective elastic properties of cracked solids: Critical review of some basic concepts", *Appl. Mech. Rev.*, **45**(8), 304-335.

Kachanov, M., Tsukrov, I. and Shafiro, B. (1994), "Effective moduli of solids with cavities of various shapes", *Appl. Mech. Rev.*, **47**(1S), S151-S174.

Kern, H. and Tubia, J.M. (1993), "Pressure and temperature dependence of P-and S-wave velocities, seismic anisotropy and density of sheared rocks from the Sierra Alpujata massif (Ronda peridotites, Southern Spain)", *Earth Planet. Sci. Lett.*, **119**(1-2), 191-205.

Korsnes, R.I., Madland, M.V., Austad, T., Haver, S. and Røsland, G. (2008), "The effects of temperature on the water weakening of chalk by seawater", *J. Petrol. Sci. Eng.*, **60**(3), 183-193.

Lamy-Chappuis, B., Angus, D., Fisher, Q.J. and Yardley, B.W. (2016), "The effect of CO_2-enriched brine injection on the mechanical properties of calcite-bearing sandstone", *Int. J. Greenhouse Gas Control*, **52**, 84-95.

Liang, W., Yang, X., Gao, H., Zhang, C., Zhao, Y. and Dusseault, M.B. (2012), "Experimental study of mechanical properties of gypsum soaked in brine", *Int. J. Rock Mech. Min. Sci.*, **53**,142-150.

Lisabeth, H.P. and Zhu, W. (2015), "Effect of temperature and pore fluid on the strength of porous limestone", *J. Geophys. Res. Solid Earth*, **120**(9), 6191-6208.

Liu, B.X., Huang, J.L., Wang, Z.Y. and Liu, L. (2009), "Study on damage evolution and acoustic emission character of coal-rock under uniaxial compression", *Chin. J. Rock Mech. Eng.*, **28**(S1), 3234-3234.

Liu, X., Wang, X., Wang, E., Liu, Z. and Xu, X. (2017), "Study on ultrasonic response to mechanical structure of coal under loading and unloading condition", *Shock Vib*.

Lu, Z.D., Chen, C.X., Feng, X.T. and Zhang, Y.L. (2014), "Strength failure and crack coalescence behavior of sandstone containing single pre-cut fissure under coupled stress, fluid flow and changing chemical environment", *J. Central South Univ.*, **21**(3), 1176-1183.

Masuda, K., Arai, T., Fujimoto, K., Takahashi, M. and Shigematsu, N. (2012), "Effect of water on weakening preceding rupture of laboratory-scale faults: Implications for long-term weakening of crustal faults", *Geophys. Res. Lett.*, **39**(1).

Nasvi, M.C.M., Ranjith, P.G., Sanjayan, J., Haque, A. and Li, X. (2014), "Mechanical behaviour of wellbore materials saturated in brine water with different salinity levels", *Energy*, **66**, 239-249.

Pei, L., Blöcher, G., Milsch, H., Deon, F., Zimmermann, G., Rühaak, W. and Huenges, E. (2016), "Thermal strain in a water-saturated limestone under hydrostatic and deviatoric stress states", *Tectonophysics*, **688**, 49-64.

Stanchits, S., Vinciguerra, S. and Dresen, G. (2006), "Ultrasonic velocities, acoustic emission characteristics and crack damage of basalt and granite", *Pure Appl. Geophys.*, **163**(5-6), 975-994.

Tang, C.A. (1993), *Catastrophe in Rock Unstable Failure*, Coal Industry Press, Beijing, China.

Vajdova, V., Baud, P. and Wong, T. (2004), "Permeability evolution during localized deformation in Bentheim sandstone", *J. Geophys. Res. Solid Earth*, **109**(B10).

Vulin, D., Kurevija, T. and Kolenkovic, I. (2012), "The effect of mechanical rock properties on CO_2 storage capacity", *Energy*, **45**(1) 512-518.

Wang, F., Cao, P., Cao, R.H., Xiong, X.G. and Hao, J. (2018), "The influence of temperature and time on water-rock interactions based on the morphology of rock joint surfaces", *Bull. Eng. Geol. Environ.*, 1-10.

Wu, J., Feng, M., Yu, B. and Han, G. (2017), "The length of pre-existing fissures effects on the mechanical properties of cracked red sandstone and strength design in engineering", *Ultrasonics*, **82**, 188-199.

Xu, T., Ranjith, P.G., Wasantha, P.L.P., Zhao, J., Tang, C.A. and Zhu, W.C. (2013), "Influence of the geometry of partially-spanning joints on mechanical properties of rock in uniaxial compression", *Eng. Geol.*, **167**(24), 134-147.

Yan, C., Deng, J., Cheng, Y., Yan, X., Yuan, J. and Deng, F. (2017), "Rock mechanics and wellbore stability in Dongfang 1-1 gas field in South China Sea", *Geomech. Eng.*, **12**(3), 465-481.

Yang, S.Q., Huang, Y.H. and Ranjith, P.G. (2018), "Failure mechanical and acoustic behavior of brine saturated-sandstone containing two pre-existing flaws under different confining pressures", *Eng. Fract. Mech.*, **193**, 108-121.

Yang, S.Q., Tian, W.L. and Huang, Y.H. (2018), "Failure mechanical behavior of pre-holed granite specimens after elevated temperature treatment by particle flow code", *Geothermics*, **72**, 124-137.

Yang, S.Q., Xu, P., Li, Y.B. and Huang, Y.H. (2017), "Experimental investigation on triaxial mechanical and permeability behavior of sandstone after exposure to different high temperature treatments", *Geothermics*, **69**, 93-109.

Yu, W.D., Liang, W.G., Li, Y.R. and Yu, Y.M. (2016), "The meso-mechanism study of gypsum rock weakening in brine solutions", *Bull. Eng. Geol. Environ.*, **75**(1), 359-367.

Zhou, H., Liu, H., Hu, D., Yang, F., Lu, J. and Zhang, F. (2016), "Anisotropies in mechanical behaviour, thermal expansion and P-wave velocity of sandstone with bedding planes", *Rock Mech. Rock Eng.*, **49**(11), 4497-4504.

Zhou, Z., Cai, X., Ma, D., Chen, L., Wang, S. and Tan, L. (2018), "Dynamic tensile properties of sandstone subjected to wetting and drying cycles", *Construct. Build. Mater.*, **182**, 215-232

CC